Biomaterials Science

ROYAL SOCIETY OF CHEMISTRY

PAPER

View Article Online
View Journal | View Issue

Open Access Article. Published on 28 September 2021. Downloaded on 1/21/2026 7:01:05 PM.
This article is licensed under a Creative Commons Attribution-NonCommercial 3.0 Unported Licence.

Check for updates

Cite this: *Biomater. Sci.*, 2021, **9**, 7492

Thermosensitive chitosan-based hydrogels supporting motor neuron-like NSC-34 cell differentiation

Antonella Stanzione,[a,b] Alessandro Polini,*[b] Velia La Pesa,[c] Angelo Quattrini,[c] Alessandro Romano,*[c] Giuseppe Gigli,[a,b] Lorenzo Moroni [b,d] and Francesca Gervaso *[b]

Motor neuron diseases are neurodegenerative diseases that predominantly affect the neuromuscular system. To date, there are no valid therapeutic treatments for such diseases, and the classical experimental models fail in faithfully reproducing the pathological mechanisms behind them. In this regard, the use of three-dimensional (3D) culture systems, which more closely reproduce the native *in vivo* environment, can be a promising approach. Hydrogel-based systems are among the most used materials to reproduce the extracellular matrix, featuring an intrinsic similarity with its physiological characteristics. In this study, we developed a thermosensitive chitosan-based hydrogel combined with β-glycerophosphate (βGP) and sodium hydrogen carbonate (SHC), which give the system optimal mechanical properties and injectability, inducing the hydrogel sol–gel transition at 37 °C. An *ad hoc* protocol for the preparation of the hydrogel was established in order to obtain a highly homogeneous system, leading to reproducible physicochemical characteristics and easy cell encapsulation. All formulations supported the viability of a neuroblastoma/spinal cord hybrid cell line (NSC-34) beyond two weeks of culture and enabled cell differentiation towards a motor neuron-like morphology, characterized by the presence of extended neurites. Based on our results, these hydrogels represent excellent candidates for establishing 3D *in vitro* models of motor neuron diseases.

Received 15th July 2021,
Accepted 23rd September 2021

DOI: 10.1039/d1bm01129d

rsc.li/biomaterials-science

Introduction

Motor neuron diseases (MNDs) encompass a heterogeneous group of neurological disorders defined and characterized by the degeneration of motor neurons.[1] Among these, amyotrophic lateral sclerosis (ALS) is the most severe form, involving both lower and upper motor neurons leading to muscle weakness, respiratory failure and, ultimately, death,[2] which occurs three to five years from the symptom onset.[1] The cause of motor neuron degeneration in ALS is still unclear.[3] Several mechanisms, however, have been proposed, including oxidative stress,[4] mitochondrial dysfunction,[5] ER stress, misfolded protein aggregation and impaired degradation,[6] neuroinflammation and RNA/DNA regulation.[7] At present, one of the limitations of translational research in ALS is that the preclinical studies have failed to predict the efficacy of new therapeutic approaches in patients.[8,9] Significant phenotypic and genotypic heterogeneity of patients, inadequate animal models and questionable relevance of the current cellular models are some of the potential reasons for the failure of clinical trials in ALS.[10,11] Research identified promising therapeutics in 2D culture cell models. However, ALS remains a disease with no effective treatment.[12,13] 2D culture models have been indisputably fundamental for increasing the knowledge on several main cellular processes and represent an indubitably economical and reproducible tool.[14] However, they have the great limitation of not being able to reproduce the three dimensionality of tissues and cellular interactions.[15–17] The physiological environment that cells experience *in vivo* is three-dimensional, as cells live in the extracellular matrix (ECM),[18,19] therefore, in the study of complex pathologies, such as MNDs, it is of paramount importance to reproduce the three-dimensionality of the tissue by means of 3D culture systems. The 3D environment, indeed, strongly influences cell fate and morphology,[20]

[a]*Dipartimento di Matematica e Fisica E. De Giorgi, University of Salento, 73100 Lecce, LE, Italy*
[b]*CNR-Nanotec, Institute of Nanotechnology, 73100 Lecce, Italy.*
E-mail: alessandro.polini@nanotec.cnr.it, francesca.gervaso@nanotec.cnr.it;
Tel: +39-0832319305
[c]*IRCCS San Raffaele Scientific Institute, Neuropathology Unit, Institute of Experimental Neurology and Division of Neuroscience, 20132 Milan, Italy.*
E-mail: romano.alessandro@hsr.it
[d]*Complex Tissue Regeneration department, MERLN Institute for Technology-Inspired Regenerative Medicine, Maastricht University, 6229 ER Maastricht, The Netherlands*

This journal is © The Royal Society of Chemistry 2021

Open Access Article. Published on 28 September 2021. Downloaded on 1/21/2026 7:01:05 PM.
This article is licensed under a Creative Commons Attribution-NonCommercial 3.0 Unported Licence.

playing a key role in all cellular processes such as proliferation,[21] differentiation,[21] migration and death.[14,22] In a 3D culture system, immortalized cells or stem cells are embedded in matrices or seeded onto previously formed scaffolds.[15,23] In this regard, hydrogels are excellent candidates for reproducing the ECM in 3D culture systems because of their high affinity to the microenvironment of most biological tissues and thanks to the ease of embedding cells inside them and obtaining homogeneous cell distribution. Defined as a "three-dimensional hydrophilic polymer network capable of absorbing and retaining large amounts of water or biological fluids",[24] hydrogels can be made of natural (*e.g.* chitosan, collagen, cellulose) or synthetic (*e.g.* polyethylene glycol acid polylactic, polyglycolic acid) polymers.[25,26] They are biocompatible and can have a highly porous structure, advantageous for the diffusion of nutrients or the release of drugs.[27–29] They can also be responsive to external stimuli, such as temperature, pH, ionic strength and electric or magnetic fields providing significant technological advantages, such as sol–gel transition, degradation and biomolecule release on demand.[30] Hydrogels responsive to pH or chemical stimuli are certainly of high interest for targeting specific anatomical compartments, but are limited in terms of responsiveness and versatility.[31] Thermoresponsive hydrogels, on the other hand, have unique characteristics in terms of biocompatibility, biodegradability and biological functionality, finding large application in the biomedical field.[32] They can be designed in order to be in the liquid phase in the temperature range of 8–25 °C and switch to the gel phase at the physiological temperature of biological fluids (36–37 °C), making them unique and suitable materials for the development of therapeutic delivery systems,[33] soft implants *in vivo*[34] and 3D *in vitro* models.[35] These characteristics are indeed tremendously appealing: they facilitate the encapsulation of target cells at room temperature and, later, allow the formation of a stable hydrogel system *in situ* at body temperature without using additional chemical or physical stimuli. Thermosensitive hydrogels can therefore overcome the typical drawbacks of traditional hydrogel culture systems that arise during the cell encapsulation step: (i) non-homogeneous cell distribution within the hydrogel due to the high viscosity of the pre-polymer solution; and (ii) cytotoxicity effects related to the use of additional chemicals or physical stimuli (*e.g.* UV exposure, application of electrical or magnetic fields, residual toxic crosslinker molecules). The second fundamental ingredient for the realization of a 3D *in vitro* system for the study of MNDs is motor neurons. In fact, a suitable 3D model consists of the perfect integration of the cellular components with the matrix.[36] NSC-34 cells produced by the fusion of a murine neuroblastoma hybrid line with motor neuron-enriched embryonic spinal cord cells are the most widely used model of immortalized motor neurons.[37] In particular, these cells can be differentiated *in vitro* to exhibit morphological and functional characteristics of primary motor neurons (such as neurite outgrowth and the expression of motor neuron specific markers)[37,38] making them a suitable model for the study of the pathophysiology of motor neurons. The ability of NSC-34 cells to differentiate into motor neurons, however, has never been tested in a 3D environment.

In this work, we synthesized a thermosensitive, injectable chitosan-based hydrogel for the encapsulation of NSC-34 cells and their motor neuron differentiation as a potential 3D *in vitro* model for the study of MNDs. Chitosan (Ch) is a natural polymer that is derived from the exoskeleton of crustaceans.[39] It is biocompatible, non-immunogenic and biodegradable[40–42] and its molecular structure makes it suitable for the reproduction of the ECM, thanks to its resemblance to glycoaminoglycans.[43] In this regard, chitosan is used in neural tissue engineering.[16,44] In our system, thermoresponsiveness of chitosan was obtained by the addition of β-glycerophosphate (βGP). The interaction of βGP with the polar chains of chitosan is the basis of the thermoresponsive effect that determines a gelation of the hydrogel in the temperature range between 32 and 37 °C, preventing the rapid precipitation of the polymer[45–47] and bringing the pH back to physiological values. In our system, in combination with βGP, sodium hydrogen carbonate (SHC) was chosen in order to increase the mechanical properties and stability, as described in the literature.[48,49] We optimized an *ad hoc* protocol for the synthesis of the hydrogel using a cold drop by drop method, which led to characteristics suitable for 3D culture. The protocol developed allowed us to obtain a bubble-free system, a very important feature not only to improve the cellular encapsulation phase but also to achieve solid physical characteristics of the hydrogel. We developed two formulations of hydrogels (Ch + βGP and Ch + βGP + SHC), which have been compared and characterized through stability, swelling, compression and diffusion tests. Furthermore, biological analyses were carried out using NSC-34 cells. In order to reproduce an *in vitro* model suitable for the study of MNDs, we encapsulated NSC-34 cells within the two formulations of hydrogels and conducted a differentiation study of the cells grown in a 3D fashion.

Materials and methods

Chitosan-based hydrogel preparation

The hydrogels (Ch + βGP and Ch + βGP + SHC) were obtained by mixing a Ch solution with two different gelling agent solutions (GA), containing βGP or βGP + SHC. The Ch solution was prepared by solubilizing 3.33 g of low molecular weight Ch powder (degree of deacetylation 75–85%, MW 50.000–190.000 Da, #448869, Sigma Aldrich, Milan, Italy) in 100 mL of 0.1 M HCl, stirred overnight at 20 °C (room temperature, r.t.) and centrifuged (2500 rpm, 5 min) to remove air bubbles. For the Ch + βGP hydrogel, the GA solution was composed of βGP only and prepared by dissolving βGP salt pentahydrate powder (MW 306.11 g mol^{-1}, #35675, Sigma Aldrich, Milan, Italy) in Milli-Q water at the initial concentration of 0.5 M (GA solution #1, Table 1). For the Ch + βGP + SHC hydrogel, SHC powder (MW 84.007 g mol^{-1}, #401676, Sigma Aldrich, Milan, Italy) was added to the abovementioned GA solution at an initial concentration of 0.125 M (GA solution #2, Table 1). The hydrogels

Open Access Article. Published on 28 September 2021. Downloaded on 1/21/2026 7:01:05 PM.
This article is licensed under a Creative Commons Attribution-NonCommercial 3.0 Unported Licence.

Table 1 pH values and concentration of gelling agent, chitosan and hydrogel solutions

Samples	Concentration			pH
	βGP	SHC	Ch	
GA solution #1 (βGP)	0.5 M	—	—	8.6
GA solution #2 (βGP + SHC)	0.5 M	0.125 M	—	8.6
Ch solution	—	—	3.33%	5.5
Ch + βGP hydrogel	0.2	—	2%	7.5
Ch + βGP + SHC hydrogel	0.2	0.05	2%	7.5

were finally obtained by adding GA solution #1 or #2 drop by drop to a cold Ch solution at a Ch : GA v/v ratio of 3 : 2, and manually mixed at 4 °C manually (drop rate of 100 μL min^{-1}). The final concentration of Ch and GA #1 and #2 are reported in Table 1. Immediately after mixing, the hydrogels were injected into plastic molds and placed in an oven at 37 °C for 2 h to induce the sol–gel thermal transition. The pH values of the different solutions and hydrogels were measured (Table 1).

Gelation time and injectability test

Injectability of the hydrogel formulations was evaluated immediately after mixing using a 23G needle at r.t. The sol–gel transition was evaluated by monitoring the gelation time by the inversion tube test. The state of "sol" or "gel" was defined by observing the flow or non-flow of the hydrogel along the walls of an inverted glass tube every 5 min at 37 °C (Fig. 1).[48]

Rheological test

The rheological properties of the hydrogels were studied using an Anton Paar instrument (Physica MCR 301, Germany) equipped with a two plate geometry (plate diameter 25 mm, gap distance 0.5 mm) and connected to a circulating water bath. Immediately following the preparation of βGP and βGP-SHC hydrogels, the variation with temperature of storage modulus (G') and loss modulus (G'') was measured in the linear viscoelastic range, at a constant shear strain (5%) and a constant frequency (1 Hz). The temperature was increased from 5 to 55 °C at a rate of 1 °C min^{-1} and the solutions were maintained at 4 °C before mixing. Each test was performed in duplicate.

Stability test and swelling ratio

Stability test was conducted in order to monitor the *in vitro* hydrogel degradation kinetics under physiological conditions in a non-enzymatic environment. The degradation profile was obtained by measuring the weight loss of the hydrogels immersed in PBS at different timepoints. The weight measurement was taken after 1, 24, 48, and 72 h, and 7, 11, 14 and 19 days. The percentage of weight loss (WL) was calculated using eqn (1):

$$\mathrm{WL}\ (\%) = (W_0 - W_i)/(W_0) \times 100 \quad (1)$$

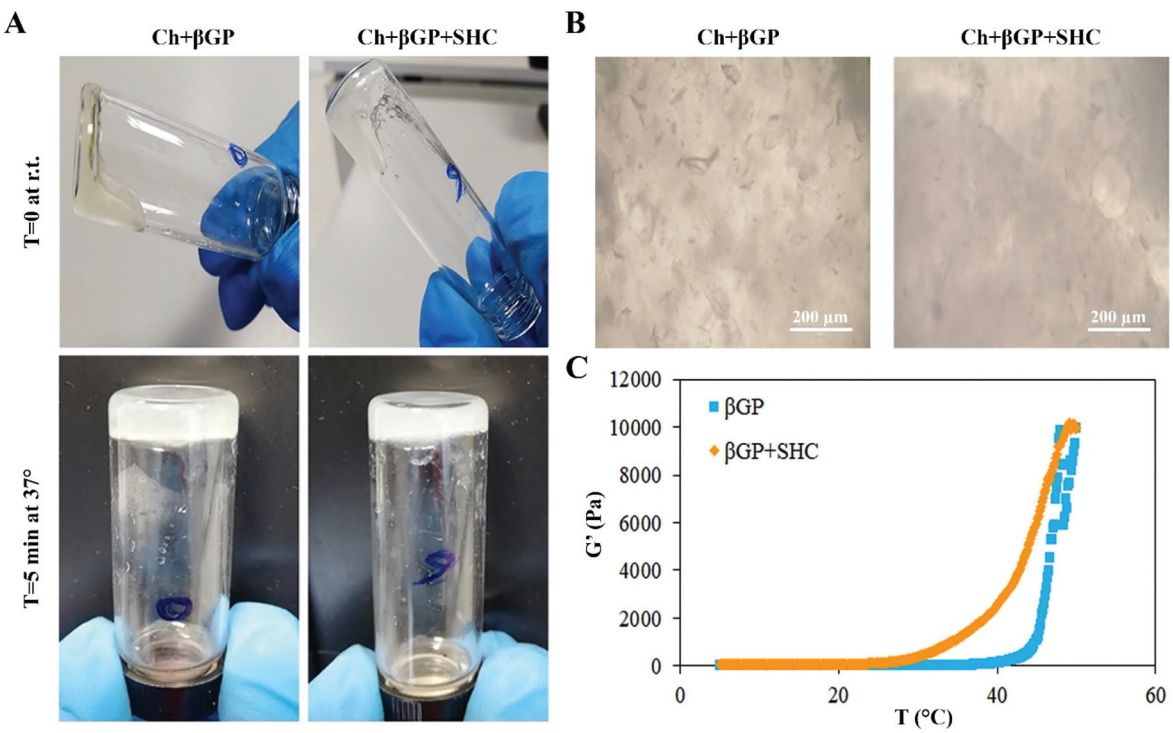

Fig. 1 (A) Inversion tube test: images of the Ch + βGP and Ch + βGP + SHC formulations taken after mixing at r.t. and after 5 min at 37 °C. (B) Optical microscopic images of the formed hydrogels. Both formulations had homogeneous texture and complete absence of bubbles. (C) Temperature dependence of the βGP and βGP-SHC hydrogels' storage modulus (G') upon heating from 5 to 55 °C at a rate of 1 °C min^{-1}.

Open Access Article. Published on 28 September 2021. Downloaded on 1/21/2026 7:01:05 PM.
This article is licensed under a Creative Commons Attribution-NonCommercial 3.0 Unported Licence.

where W_0 is the weight of the hydrogel after thermal gelation at 37 °C and W_i is the weight at the different selected timepoints.

The degree of swelling of the hydrogel was obtained by monitoring the weight of the hydrogels immersed in PBS at 37 °C at different timepoints: 10, 20, and 30 min, and 1, 2, 4, 6, 24, 48, 72 and 96 h. Freeze-dried hydrogels were weighed before and after hydration. The swelling ratio percentage (SR) was calculated according to eqn (2):

$$\mathrm{SR}\ (\%) = [(W_{\mathrm{wet}} - W_{\mathrm{dry}})/W_{\mathrm{dry}}] \times 100. \quad (2)$$

Compression test

Compression test was carried out to determine the stiffness of the hydrogels. The samples were tested 2 h after gelation at r.t. and in wet conditions (*i.e.* immersed in PBS). A universal testing machine (ZwickiLine 1kN, Zwick Roell, Kennesaw, GA, USA) with a 10 N load cell was used. The test was conducted up to 75% deformation and with a displacement velocity of 2 mm min^{-1}. In order to evaluate the non-linearity of the hydrogel stiffness, the Young's secant modulus, considered as the slope of a line connecting the point of zero strain to a point at a specified deformation, was calculated up to 50% and plotted.

Scanning electron microscopy (SEM) analysis

The two types of hydrogels were observed by scanning electron microscopy (SEM EVO 40, Carl Zeiss AG, Oberkochen, Germany) to investigate the porosity of the systems. The samples were freeze-dried and cut to obtain longitudinal and transverse sections. Before the SEM visualization, the samples were gold coated (thickness 10 nm; CCU-010 HV, Safematic GmbH, Zizers, Switzerland). The images were acquired at different magnifications using an accelerating voltage of 5 kV. Pore dimension was evaluated by analyzing at least 200 pores from five SEM images per each hydrogel type using the ImageJ software (v. 1.8.0_172).

Permeability test

The permeability test was conducted in order to evaluate the diffusion through the hydrogels of nutrients and small proteins[50] using three different fluorescein isothiocyanate–dextran (FD) molecules (Sigma Aldrich) of different molecular weights (3–5 kDa, 10 kDa and 70 kDa). The samples were prepared by injecting 1.5 mL of each formulation of hydrogel into glass vials (diameter 15 mm) and incubated in an oven at 37 °C for 30 min. After incubation, 1 mL of FD-3–5 or FD-10 or FD-70 solution prepared in PBS at a concentration of 1 mg mL^{-1} was added to each hydrogel formulation. The samples were then incubated at 37 °C and at different timepoints (1, 6 and 24 h) the absorbance at 490 nm was read to quantify the residual dextran concentration in the supernatant (*i.e.* calculating the amount of FD in the hydrogel indirectly). At the same time, the diffusion of dextran in the hydrogel at the different timepoints was observed by visual inspection by monitoring the color change of the samples.

Cell culture and cell encapsulation in hydrogel

The motor neuron-like NSC-34 cell line was a gift from Dario Bonanomi (San Raffaele Scientific Institute, Milan, Italy). Cells were cultured in Dulbecco's Modified Eagle Medium (DMEM) with 2 mM glutamine (Corning, New York, US) supplemented with 10% FBS, 100 U mL^{-1} penicillin and 100 g mL^{-1} streptomycin (Corning). Cells were incubated at 37 °C with 95% of humidity and 5% of CO_2. 2×10^6 cells were removed, centrifuged for 5 min at 1200 rpm and the pellet was suspended in 100 μL of DMEM. The resulting cell suspension was added to 1 mL of a hydrogel (at the sol phase) by gently mixing with a spatula in order to homogeneously distribute the cells. Drops (50 μL) of cell-laden hydrogels were placed in a 24-well cell culture plate at 37 °C in order to induce the sol–gel transition of the thermosensitive hydrogels. After 10 min, complete DMEM (500 μL) was finally added to each well.

Live and dead assay

The live and dead assay was conducted to evaluate the viability of NSC-34 cells in the hydrogels. Assays were performed using 100 μL drops of cell-embedded hydrogels and the cell viability was evaluated at three timepoints: 1, 3 and 7 days. Live and dead cells in hydrogel were detected using the ReadyProbes cell viability imaging kit, Blue/Red (Invitrogen, Milan, Italy), following the protocol suggested by the manufacturer. The working solution was prepared by adding 2 drops of NucBlue Live reagent and 2 drops of propidium iodide to each mL of culture medium. The samples were deprived of the medium, washed 3 times with PBS, covered with the working solution and incubated at 37 °C for 2 h in the dark. At the end of the incubation time, the samples were washed with PBS and the images were acquired under fluorescence microscopy (Axio Zoom.V16, Zeiss, Oberkochen, Germany) at 360 nm for NucBlue® Live reagent (live cells) and 535 nm for propidium iodide (dead cells).

Presto Blue assay

In order to evaluate the metabolism of the cells encapsulated in the hydrogels, the Presto Blue (Invitrogen) test was performed at 1, 4, and 8 days. The samples were deprived of the culture medium and replaced with the culture medium added with the reagent from the Presto Blue kit at 1× concentration. The samples were incubated in the incubator for 2 h in the dark. At the end of the incubation time, the medium was recovered and the absorbance at 570 nm was read, using the wavelength of 600 nm as the reference. Data were expressed as a percentage of metabolic activity and all the results were normalized to day 1 values.

Differentiation of hydrogel-encapsulated NSC-34 cells

For differentiation studies, 100 μL of hydrogels with embedded NSC-34 cells (2×10^6 cells per mL of hydrogel) were deposited on the surface of a 24-well plate to create thin films. NSC-34

Open Access Article. Published on 28 September 2021. Downloaded on 1/21/2026 7:01:05 PM.
This article is licensed under a Creative Commons Attribution-NonCommercial 3.0 Unported Licence.

cells encapsulated in hydrogels were kept in a proliferative medium (DMEM, 10% FCS, 0.5% P/S) for 4 days. After 4 days, the culture medium was replaced with a differentiation medium containing 1 : 1 DMEM/F-12 (Ham), 1% FCS, 1% modified Eagle's medium with non-essential amino acids (NEAA), 0.5%/S and all-*trans* retinoic acid at a final concentration of 10 μM as reported in the literature.[51] Cells were kept in culture for 8 days and the differentiation medium was changed every 2 days.[52] NSC-34-laden hydrogels maintained for 8 days in normal proliferative medium was used as the control.

Analysis of cell morphology and cell distribution in hydrogels

In order to evaluate the morphology and distribution of the NSC-34 cells encapsulated in the hydrogels before and after differentiation, DAPI–phalloidin staining was performed as follows: samples were fixed in 4% PFA in PBS for 20 min, permeabilized with Triton X-100 in PBS, incubated with 1% BSA in PBS for 1 h, stained with phalloidin–FITC in PBS (1 : 400 v/v) (Sigma Aldrich) and incubated with DAPI (nuclei) solution in PBS (1 : 10 000 v/v). The distribution of cells in the hydrogels was evaluated by observation of the samples under a confocal microscope (Leica TCS SP8 STED, Leica Microsystems, Wetzlar, Germany), using a *Z*-stack thickness of 100 μm.

Immunofluorescence staining

NSC-34 cells differentiated in the hydrogels were analyzed by immunofluorescence microscopy. Samples were fixed in 4% PFA in PBS for 20 min, permeabilized with Triton X-100 in PBS, incubated with 1% BSA in PBS for 1 h and then with the primary anti-neurofilament H non-phosphorylated mouse mAb antibody SMI-32 (Sigma Aldrich) in 1% BSA in PBS (1 : 1000 v/v) overnight at 4 °C. Afterwards, the samples were incubated with a secondary antibody, goat anti-mouse IgG (H + L) conjugated with Alexa Fluor 555 (Sigma Aldrich), in 1% BSA in PBS (1 : 1000 v/v) for 1 h, stained with phalloidin–FITC in PBS (1 : 400 v/v) (Sigma Aldrich) and incubated with DAPI solution in PBS (1 : 10 000 v/v). The images were acquired by fluorescence microscopy (Nikon Eclipse Ti).

Neurite outgrowth analysis

Neurite outgrowth/elongation was determined by image analysis at the end of cell differentiation after immunostaining for neurofilaments using manual tracing of images. At least 10 images were taken for each sample in order to have a sufficient number of neurites to support the statistical analysis. For each formulation of cell-laden hydrogels, three different parameters were analyzed (Table 2).

Table 2 Parameters of neurite outgrowth analyzed by image analysis

Parameters	Description
Cells developing neurites	Number of cells displaying neurites from cell body
Number of branches	Number of branches per cell body
Neurite length	Total length (μm) of neurites

Statistical analysis

All the experiments were performed in triplicate, unless otherwise indicated. The results of multiple observations are shown as the average value ± the mean standard deviation. Student's *t*-test was used to evaluate the significance of the data. The values were considered significant with $p < 0.05$.

Results

Two hydrogel formulations, Ch + βGP and Ch + βGP + SHC, were successfully prepared according to the optimized protocol that led to obtaining a bubble-free system. The feasibility of using the two developed hydrogels as a 3D cell-embedding system has been verified by performing chemical, physical and biological characterization.

pH value measurements

The pH values of Ch and GA were measured before mixing and again after the formation of the hydrogel. The values, reported in Table 2, show that after mixing both types of hydrogels (Ch + βGP and Ch + βGP + SHC) had physiological pH values compatible with cell viability.

Thermosensitivity and injectability of hydrogels

The thermoresponsiveness of the βGP and βGP + SHC hydrogels was first assessed by the inversion tube test. All samples flowed along the walls of the vial immediately after mixing at r. t. while they stopped to flow after a few min at 37 °C highlighting the transition from the sol to the gel state (Fig. 1A). Injectability was demonstrated through the passage of both hydrogel formulations, immediately after mixing, through a 23G needle. After polymerization, the hydrogel appeared homogeneous and bubble-free (Fig. 1B), suitable for easy optical microscopic investigation during cell culture studies. Moreover, the influence of temperature on the rheological properties of the hydrogels was studied by heating samples from 5 to 55 °C at a rate of 1 °C min^{-1}, at a constant shear strain and frequency. The temperature dependence of the βGP and βGP + SHC hydrogels storage modulus (G') is reported in Fig. 1C.

Upon heating from 5 to 55 °C, the temperature at which G' rapidly increases and the slope of this increase gives an indication of the temperature of incipient gelation.[45] As can be observed in Fig. 1C, G' increased much more rapidly in hydrogels containing only βGP than in the βGP + SHC hydrogels and this increase took place at a temperature >40 °C. In the βGP + SHC hydrogels, conversely, G' started to increase remarkably at lower temperatures (>30 °C) probably because of SHC addition in the hydrogel formulation that enlarges the temperature gelation range.

Stability test and swelling ratio

The degradation profile of the hydrogels was evaluated by measuring the weight loss of the hydrogels immersed in PBS at different timepoints (Fig. 2A). Both formulations of hydrogels showed high stability over time up to 11 days and 19 days

 This journal is © The Royal Society of Chemistry 2021

Open Access Article. Published on 28 September 2021. Downloaded on 1/21/2026 7:01:05 PM.
This article is licensed under a Creative Commons Attribution-NonCommercial 3.0 Unported Licence.

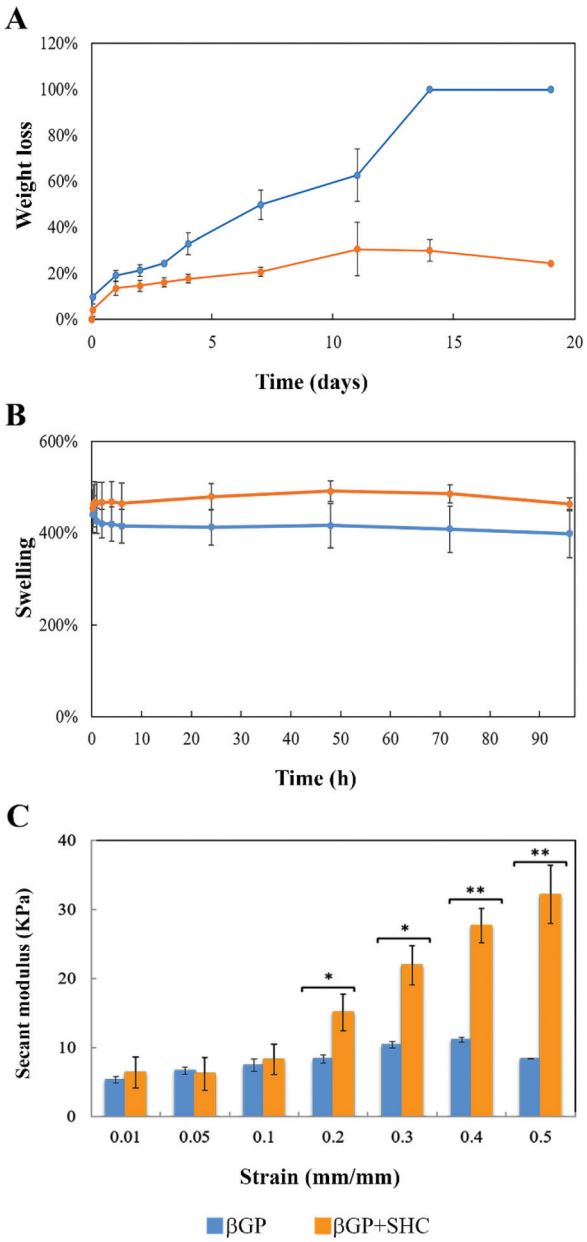

Fig. 2 (A) Stability test: weight loss trend of the two hydrogel formulations immersed in PBS at 37 °C. (B) Swelling ratio percentage of the hydrogels in PBS. (C) Secant modulus considered as the slope of a line connecting the point of zero strain to a point at a specified deformation from the stress–strain compression test performed on Ch + βGP and Ch + βGP + SHC. *$p < 0.05$, **$p < 0.01$.

for Ch + βGP and Ch + βGP + SHC, respectively. We observed a peak weight loss at day 11 for the Ch + βGP formulation, with a loss of 63% ± 11.34%, while the Ch + βGP + SHC formulation had a constant profile over time. The evaluation of the swelling of the hydrogels was obtained by weighing the samples, previously freeze-dried, before and after hydration in PBS at different timepoints. Both the formulations (Ch + βGP and Ch + βGP + SHC) reached their maximum swelling capability within the first 30 min (swelling ratio 451% ± 29% and 466% ± 45% for Ch + βGP and Ch + βGP + SHC, respectively). Furthermore, both formulations exhibited a similar swelling profile (Fig. 2B).

Compression test

The mechanical test results are reported in Fig. 2C. The Young's modulus obtained during unconfined compression at low strain values, 0–1% and 0–5% was about 6 kPa for both βGP and βGP-SHC samples, without any significant difference. However, as the strain increased (up to 50% deformation), the secant Young's modulus of βGP + SHC hydrogels becomes significantly higher than for βGP ones, indicating that the addition of SHC is a key factor in increasing the resistance of the hydrogels at strain values above 10%.

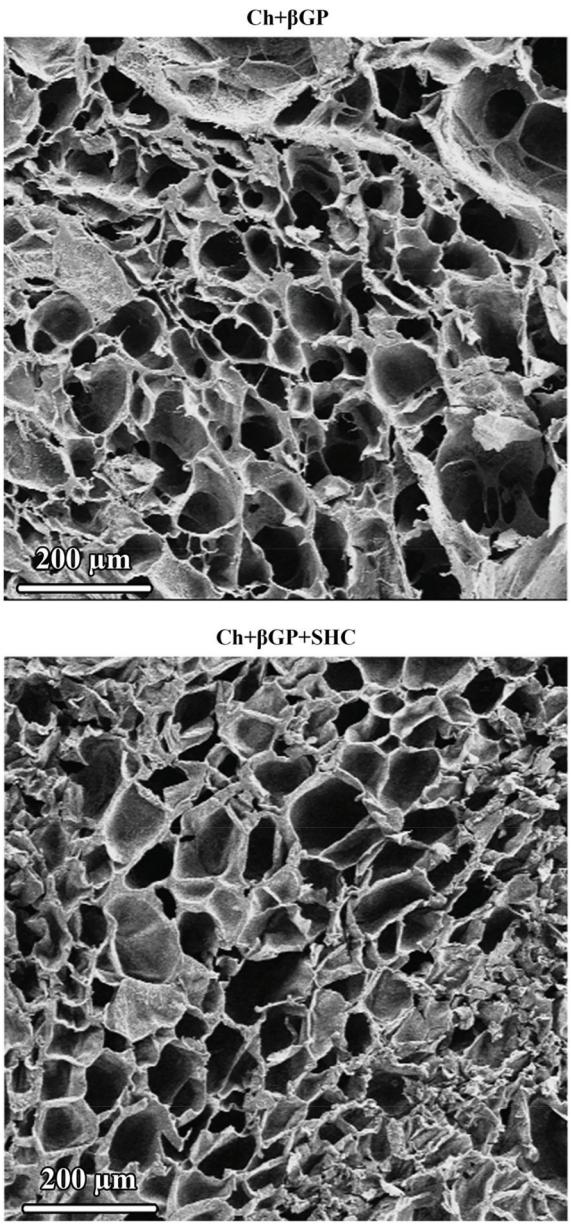

Fig. 3 SEM images of transverse and longitudinal hydrogel sections.

Open Access Article. Published on 28 September 2021. Downloaded on 1/21/2026 7:01:05 PM.
This article is licensed under a Creative Commons Attribution-NonCommercial 3.0 Unported Licence.

SEM

From the SEM observation of transverse and longitudinal sections of the hydrogel samples, both formulations showed possessing high porosity (Fig. 3), having a structure potentially permissive to the passage of nutrients and the release of catabolites and, therefore, suitable for cell encapsulation. Both types of hydrogels showed an apparent open porous structure with a pore size of (92.9 ± 31.0) μm and (92.7 ± 21.2) μm for Ch + βGP and Ch + βGP + SHC hydrogel, respectively.

Permeability test

In order to evaluate the diffusion within the hydrogels of nutrients and small proteins, a permeability experiment was conducted using FITC-labeled dextran at different molecular weights (3–5 kDa, 10 kDa and 70 kDa). The absorption of dextran within the hydrogels was calculated indirectly, by reading the fluorescence intensity of the residual dextran solution at different timepoints (Fig. 4B). At 24 h of incubation, we observed a passage of 62%, 78% and 61% of FD-3–5, FD10 and FD70, respectively for the Ch + βGP formulation, with respect to the equilibrium condition. For the Ch + βGP + SHC formulation, the passage reached 76%, 78% and 66% of FD-3–5, FD10 and FD70, respectively. The results generally showed optimal diffusion of the molecules in both formulations, confirming their potential use of encapsulating cells within the hydrogels. In particular, the Ch + βGP + SHC formulation showed a more homogeneous and linear trend of the diffused FD within it, probably reflecting its greater structural stability and a minimal degradation profile. The hydrogels absorbing the solution over time showed a visible color change, confirming the absorption of the dextran molecules (Fig. 4A).

Cell viability/proliferation in hydrogels

The viability of non-differentiated NSC-34 cells encapsulated in the hydrogels was analyzed by live and dead cell assay at 1, 4 and 7 days after culturing (Fig. 5A). NSC-34 cells spread in both hydrogel formulations and were viable up to day 7 of cell culture. In all the samples, only rare dead cells (red nuclei) were detected confirming that the hydrogel and/or its components did not elicit any cytotoxic effect towards the cells embedded. The proliferation of NSC-34 cells was evaluated using the Presto Blue metabolic assay up to 14 days (Fig. 5B). The proliferation/metabolic activity of NSC-34 cells increased and reached the maximum at day 4. The mitochondrial activity was maintained at 8 days and showed only a slight decrease at 14 days (~85% relative to the values measured at day 1). Overall, these data suggest that both hydrogels provide a suitable microenvironment to support NSC-34 cell growth.

Analysis of the NSC-34 cells differentiation in hydrogels

Fluorescence microscopy was employed to examine cell distribution within the hydrogels and to evaluate the ability of the Ch + βGP and Ch + βGP + SHC hydrogels to support NSC-34 cell differentiation (Fig. 6). NSC-34 cells encapsulated in hydrogel drops were subjected to differentiation for 8 days and then

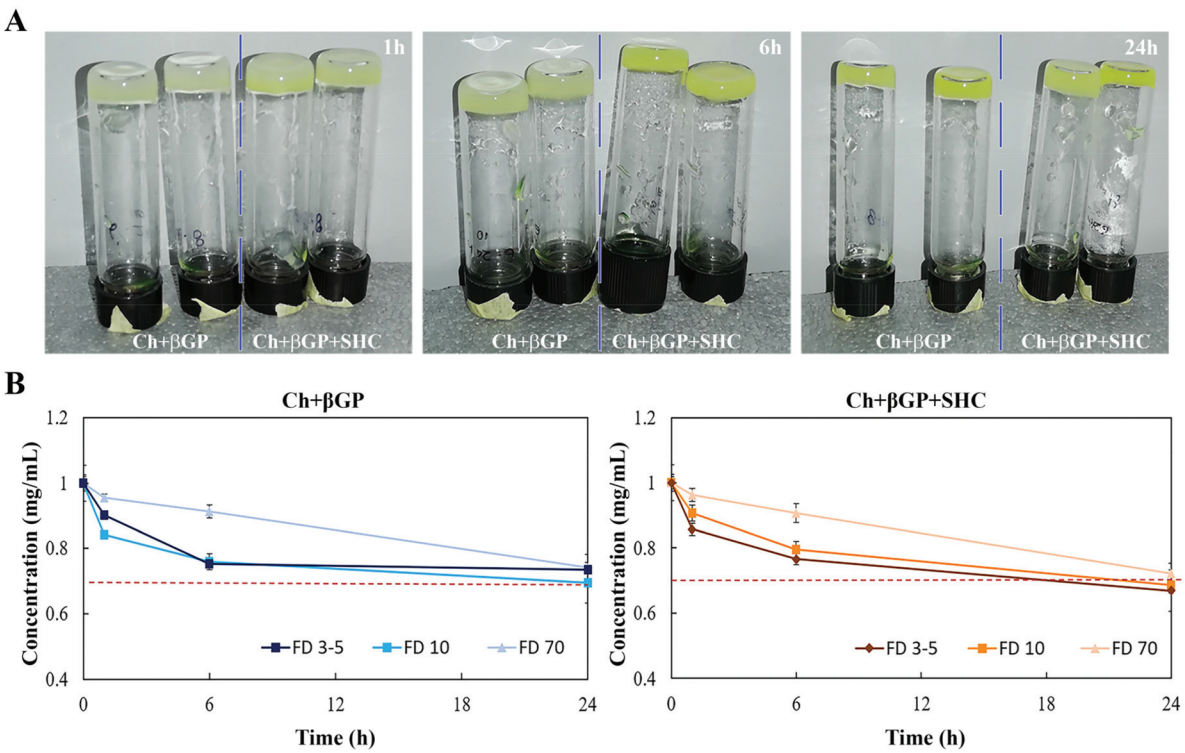

Fig. 4 (A) Representative images of the absorption of the dextran molecules in the hydrogels. (B) Graph plots reporting the absorption percentage of the FD3–5, FD10, FD70 molecules in Ch + βGP and Ch + βGP + SHC hydrogels at different timepoints.

Open Access Article. Published on 28 September 2021. Downloaded on 1/21/2026 7:01:05 PM.
This article is licensed under a Creative Commons Attribution-NonCommercial 3.0 Unported Licence.

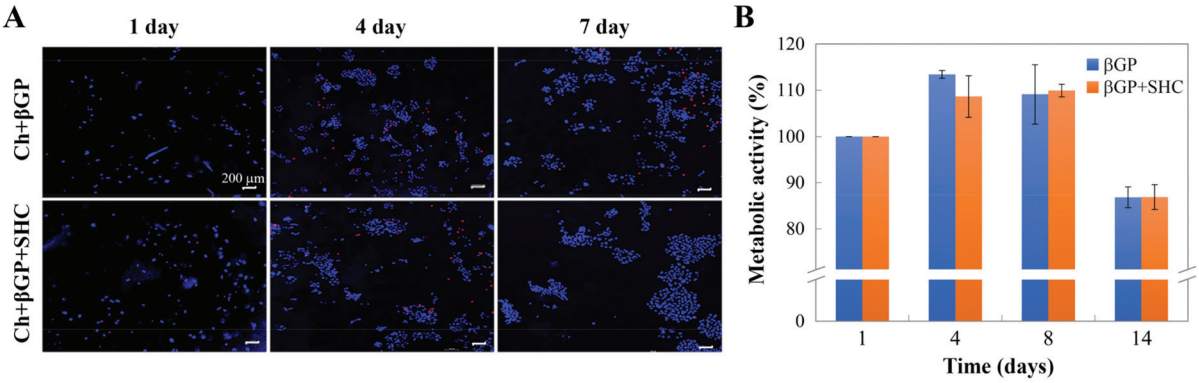

Fig. 5 (A) Live/dead assay: viability analysis of NSC-34 encapsulated cells in both hydrogel formulations up to day 7 of culturing. Blue signals refer to living cells, red signals to dead cells. (B) Presto Blue assay: metabolic activity percentage of NSC-34 cells encapsulated in Ch + βGP and Ch + βGP + SHC up to 14 days of culturing.

fixed. The three-dimensional distribution of NSC-34 cells within the hydrogels was analyzed, after DAPI/phalloidin staining, by confocal microscopy. The cells were homogeneously distributed throughout the entire hydrogel thickness and exhibited extensive neurites (Fig. 6A). The capability of NSC-34 embedded in the hydrogels to differentiate was evaluated by immunofluorescence staining using non-phosphorylated neurofilament-H (SMI-32) as the neuronal marker. Cells maintained in proliferative medium showed a rounded shape and absence of neurites (Fig. 6B). On the other hand, NSC-34 cell subject to differentiation for 8 days showed an elongated shape, neurite outgrowth and increased expression of neurofilament-H in both hydrogel formulations (Fig. 6C). To investigate the effect of the two hydrogel formulations on neurite outgrowth, three different neurite parameters (Table 2) were analyzed in the NSC-34 cells after 8 days of differentiation (Fig. 7). NSC-34 cells differentiated in the Ch + βGP + SHC hydrogel showed a greater number of neurites (Fig. 7A; 0.54 ± 10 *vs.* 0.38 ± 11) and neurite branches (15 *vs.* 8), and established longer neurite (Fig. 7C) than cells grown in the Ch + βGP hydrogels.

Discussion

In this work, we developed a thermosensitive chitosan-based hydrogel capable of homogeneously embedding neuronal cells and support their growth and differentiation in morphological terms. Although thermosensitive chitosan-based hydrogels have already been proposed for cell encapsulation,[47,53,54] here we developed an *ad hoc* preparation method for chitosan hydrogels resulting in a highly optimized system, suitable for cell encapsulation and 3D culture systems up to 8 days. The cold drop-by-drop method, used to mix chitosan and gelling agent solutions, led us to a bubble-free and much less viscous mix than the conventional Luer lock-based hydrogel system. The optimization of the molar ratios between Ch and βGP allowed the introduction of the Ch + βGP formulation not obtainable with previous methods,[50] permitting to compare the Ch + βGP and Ch + βGP + SHC formulations in chemical–physical and biological terms. The resulting system was finely tunable in terms of rheological and compressive properties, without altering the overall physico-chemical features. Both formulations were injectable at r.t. and underwent the transition from the state of "sol" to "gel" by increasing the temperature to 37 °C, a value suitable for cell viability.[55]

This feature makes our hydrogel system suitable for a number of biomedical applications, including *in vivo* regenerative medicine products and *in vitro* 3D cell culture models. The polymerization kinetics of the system, induced by simple switching to body temperature, highlight its great advantage in terms of r.t. handling, cell encapsulation and distribution over other hydrogel systems that undergo sol–gel transition out of the physiological temperature and pH range. The transition to the solid state was likely due to the establishment of hydrophobic interactions between the Ch and the βGP and the reduction of the polarity of the Ch chains.[45–47] The rheological analysis confirmed the qualitative macroscopic evaluation performed through the inversion tube test. By means of a temperature sweep test (in the range 5–55 °C), it was possible to assess that the hydrogels' storage modulus G' drastically increased as the temperature reached a value above 30 °C, demonstrating that both the βGP and βGP + SHC hydrogels show a thermosensitive response. Though, the addition of SHC to the system triggered the sol–gel transition at lower temperatures leading to a wider temperature range of gelling kinetics in comparison to the βGP system. Indeed, hydrogels with only βGP showed a more defined *on–off* temperature-based behavior, suggesting that the proposed βGP formulation could be successfully used also as a bioink in bioprinting technology. Bioinks that allow processing in a physiological environment and do not need post-processing are extremely promising in building cell-laden 3D structures.[56] The degradation kinetics revealed a high stability of the hydrogels in a hydrophilic environment and in particular the Ch + βGP + SHC formulation showed a stability up to 3 weeks in culture conditions. This enhanced stability was probably supported by

Open Access Article. Published on 28 September 2021. Downloaded on 1/21/2026 7:01:05 PM.
This article is licensed under a Creative Commons Attribution-NonCommercial 3.0 Unported Licence.

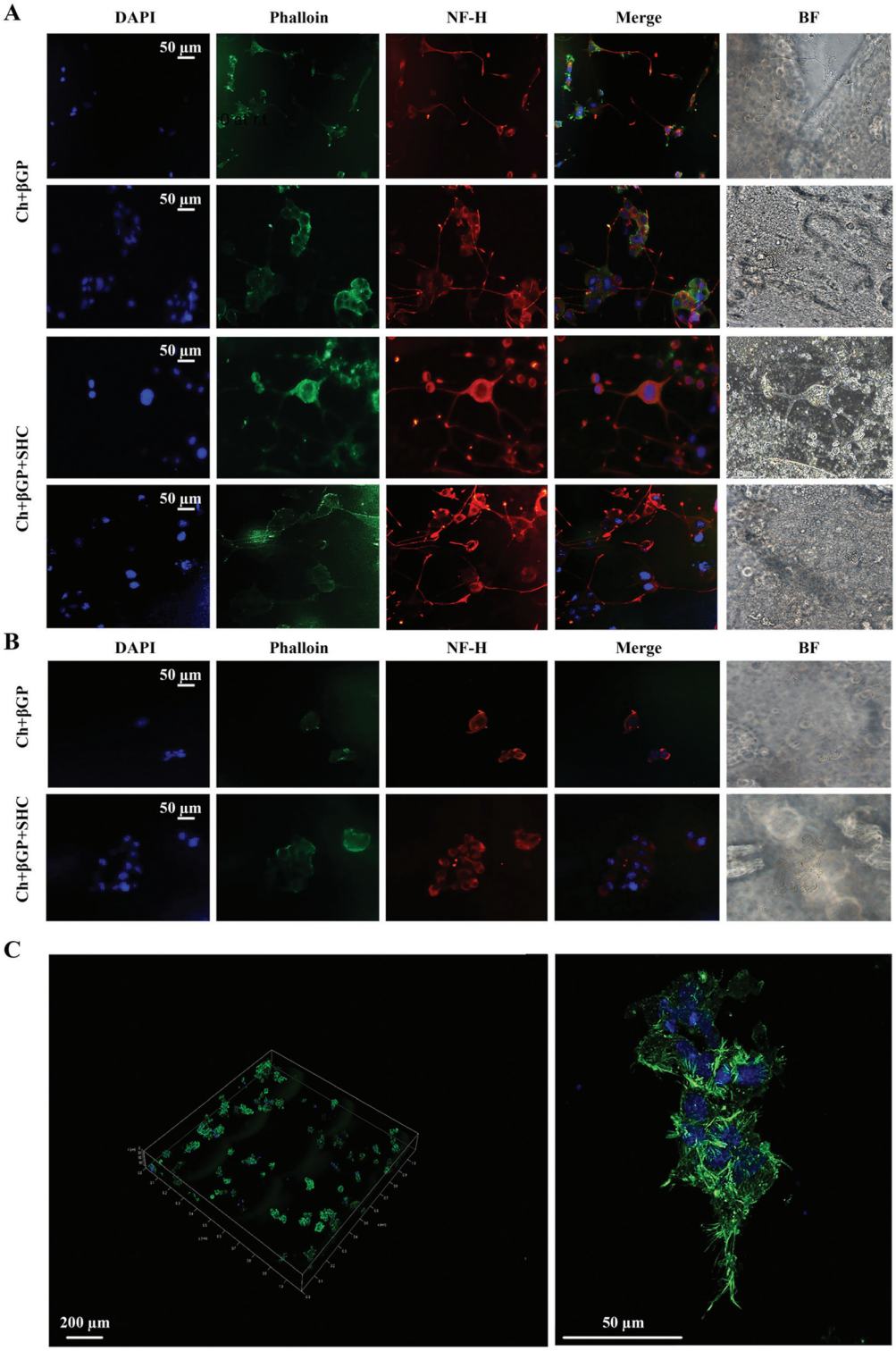

Fig. 6 (A) Immunofluorescence observation of NSC-34 cells encapsulated in Ch + βGP and Ch + βGP + SHC after 8 days of differentiation. The cells were labeled with DAPI (nuclei), phalloidin (actin) and heavy non-phosphorylated neurofilament for the evaluation of neurite elongation. In both the formulations, the cells showed an elongated morphology and the development of neurites. (B) NSC-34 cells, encapsulated in Ch + βGP and Ch + βGP + SHC and maintained for 8 days in proliferative medium, did not develop neurites and maintained a round shape. (C) Distribution of 3D cells in hydrogels and visualized by *Z*-stack and DAPI–phalloidin staining (left); detail of the cell morphology (right).

 This journal is © The Royal Society of Chemistry 2021

Open Access Article. Published on 28 September 2021. Downloaded on 1/21/2026 7:01:05 PM.
This article is licensed under a Creative Commons Attribution-NonCommercial 3.0 Unported Licence.

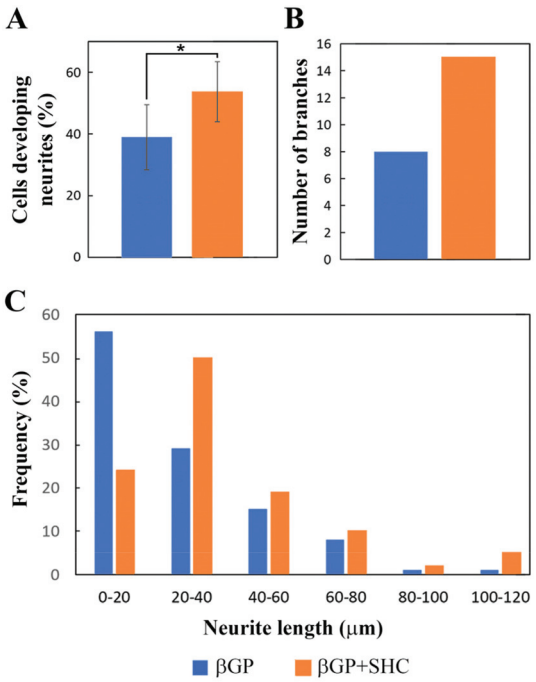

Fig. 7 (A) Plot of the percentage of cells developing neurites in Ch + βGP and Ch + βGP + SHC after 8 days of differentiation (*$p < 0.05$). (B) Total number of branch points developed by the cells in both formulations. (C) Comparison of the distribution of neurites for different length ranges.

the generation of stronger intermolecular interactions, facilitated by the presence of two GAs.[48,57] The typical superabsorbent feature of hydrogels, necessary in 3D culture systems, is confirmed by the swelling test which showed SR% values in the range of 400–600% for both formulations, in agreement with the literature.[58] The addition of SHC, in combination with βGP, was reported to increase the mechanical properties of the hydrogels.[48,49] Here, the compression tests confirmed this trend, highlighting a different mechanical profile between the two formulations.

The Ch + βGP + SHC hydrogel showed greater strength than Ch + βGP, but still in the range of "soft" biological tissues (1–10 kPa).[59] One of the fundamental requirements for a hydrogel to be used in cell culture systems is to possess a certain degree of porosity that can simultaneously guarantee the entrapment of cells and the diffusion of nutrients inside. The images obtained by SEM highlighted the internal structure of the hydrogels, which show for both the formulations open porosity with pores in the size of 92.9 ± 31.0 and 92.7 ± 21.2 for Ch + βGP and Ch + βGP + SHC samples, respectively.

Furthermore, the permeability tests confirmed that both formulations guarantee a robust supply of nutrients to the encapsulated cells, as demonstrated by the diffusion of the tested molecules over 70%. With respect to the suitability of these systems for 3D cell culture studies, NSC-34 cells showed high viability up to day 7 of culture with the presence of very rare red nuclei. The metabolic activity of the cells was also well preserved up to 8 days of culture showing only a small reduction in proliferation at a later stage (14 days). Finally, Ch + βGP and Ch + βGP + SHC were able to support the differentiation of NSC-34 cells. In particular, cells encapsulated in the hydrogels could be efficiently differentiated as motor neurons adopting standard protocols,[52] as observed after cell staining with a neuronal maker, such as the neurofilament-H. Both types of the analyzed hydrogels allowed NSC-34 cells to acquire the typical neuron-like morphology characterized by an elongated cell shape and the development of long neurites. Interestingly, the two hydrogels differently modulated neurite outgrowth of NSC-34 cells with the Ch + βGP + SHC hydrogels supporting the differentiation of cells with a greater number of neurites/branches and longer neurites than the Ch + βGP hydrogel.

Conclusions

Overall, in this study we proposed a thermosensitive chitosan-based hydrogel, prepared by implementing an innovative procedure that allowed to obtain a bubble-free system with optimal chemical–physical characteristics for use in 3D culture systems. In particular, both the developed formulations reproduce the mechanical characteristics of "soft" biological tissues,[59] a fundamental requirement for the envisioned application. Indeed, biological analyses conducted with motor neuron-like NSC-34 cells revealed the high ability of our systems to support not only cell growth and viability but also the changes in morphology induced by differentiation. Therefore, our hydrogels can be valid candidates as ECM-like biomaterials for 3D *in vitro* models to study motor neuron diseases.

Author contributions

Conceptualization, F. G., L. M., A. P. and A. R.; methodology, A. S.; hydrogel preparation, swelling, stability and permeability tests, cell encapsulation and biological investigation, A. S.; compression tests, result analysis, F. G.; supervision of cell study, contribution to analysis of the biological results, V. L. P., A. R. and A. Q.; writing – original draft preparation, A. S. and F. G.; writing – review and editing, A. P., A. R., A. Q. and L. M.; supervision, G. G., L. M. and A. Q.; funding acquisition, G. G. and A. P. All the authors have read and agreed to the published version of the manuscript.

Conflicts of interest

The authors declare no conflict of interest. The funders had no role in the design of the study; in the collection, analyses, or interpretation of data; in the writing of the manuscript, or in the decision to publish the results.

Open Access Article. Published on 28 September 2021. Downloaded on 1/21/2026 7:01:05 PM.
This article is licensed under a Creative Commons Attribution-NonCommercial 3.0 Unported Licence.

Acknowledgements

The authors are grateful to the "Tecnopolo per la medicina di precisione" (TecnoMed Puglia) - Regione Puglia: DGR n.2117 del 21/11/2018, CUP: B84I18000540002 and "Tecnopolo di Nanotecnologia e Fotonica per la medicina di precisione" (TECNOMED) - FISR/MIUR-CNR: delibera CIPE n.3449 del 7-08-2017, CUP: B83B17000010001. A. P. and F. G. gratefully acknowledge the support from the European Union's Horizon 2020 research and innovation programme under grant agreement No. 953121 (FLAMIN-GO).

Notes and references

1 D. W. Mulder, L. T. Kurland, K. P. Offord and M. Beard, *Neurology*, 1986, **36**, 511–517.
2 L. C. Wijesekera and P. N. Leigh, *Orphanet J. Rare Dis.*, 2009, **4**, 1–22.
3 P. Shaw, *J. Neurol., Neurosurg. Psychiatry*, 2005, **76**, 1046.
4 P. J. Shaw, P. G. Ince, G. Falkous and D. Mantle, *Ann. Neurol.*, 1995, **38**, 691–695.
5 L. Siklós, J. Engelhardt, Y. Harati, R. Glenn Smith, F. Joó and S. H. Appel, *Ann. Neurol.*, 1996, **39**, 203–216.
6 M. Corbo and A. P. Hays, *J. Neuropathol. Exp. Neurol.*, 1992, **51**, 531–537.
7 D. Troost, J. J. van den Oord and J. M. de Jong, *Neuropathol. Appl. Neurobiol.*, 1990, **16**, 401–410.
8 M. Benatar, *Neurobiol. Dis.*, 2007, **26**, 1–13.
9 J. L. Cummings, T. Morstorf and K. Zhong, *Alzheimer's Res. Ther.*, 2014, **6**, 1–7.
10 J. L. Elliott, *Neurobiol. Dis.*, 1999, **6**, 310–320.
11 Y. Tanaka and N. Hirokawa, *Trends Genet.*, 2002, 18.
12 P. M. Bridge, D. J. Ball, S. E. Mackinnon, Y. Nakao, K. Brandt, D. A. Hunter and C. Hertl, *Exp. Neurol.*, 1994, **127**, 284–290.
13 G. A. Robinson and R. D. Madison, *Exp. Neurol.*, 2006, **197**, 341–346.
14 H. Baharvand, S. M. Hashemi, S. K. Ashtiani and A. Farrokhi, *Int. J. Dev. Biol.*, 2006, **50**, 645–652.
15 D. Anton, H. Burckel, E. Josset and G. Noel, *Int. J. Mol. Sci.*, 2015, **16**, 5517–5527.
16 B. Morrison, D. K. Cullen and M. LaPlaca, *Stud. Mechanobiol., Tissue Eng. Biomater.*, 2011, **3**, 247–285.
17 D. Avossa, M. Grandolfo, F. Mazzarol, M. Zatta and L. Ballerini, *Neuroscience*, 2006, **138**, 1179–1194.
18 V. M. Weaver, O. W. Petersen, F. Wang, C. A. Larabell, P. Briand, C. Damsky and M. J. Bissell, *J. Cell Biol.*, 1997, **137**, 231–245.
19 A. Birgersdotter, R. Sandberg and I. Ernberg, *Semin. Cancer Biol.*, 2005, **15**, 405–412.
20 C. P. Soares, V. Midlej, M. E. W. de Oliveira, M. Benchimol, M. L. Costa and C. Mermelstein, *PLoS One*, 2012, **7**, e38147.
21 T. B. Rodrigues and P. Ballesteros, *J. Neurosci. Res.*, 2007, **3253**, 3244–3253.
22 P. D. Benya and J. D. Shaffer, *Cell*, 1982, **30**, 215–224.
23 R. Langer and D. A. Tirrell, *Nature*, 2004, **428**, 487–492.
24 A. S. Hoffman, *Adv. Drug Delivery Rev.*, 2012, **64**, 18–23.
25 A. M. Hopkins, L. De Laporte, F. Tortelli, E. Spedden, C. Staii, T. J. Atherton, J. A. Hubbell and D. L. Kaplan, *Adv. Funct. Mater.*, 2013, **23**, 5140–5149.
26 J. P. Frampton, M. R. Hynd, M. L. Shuler and W. Shain, *Biomed. Mater.*, 2011, **6**, 015002.
27 D. Buenger, F. Topuz and J. Groll, *Prog. Polym. Sci.*, 2012, **37**, 1678–1719.
28 L. Klouda and A. G. Mikos, *Eur. J. Pharm. Biopharm.*, 2008, **68**, 34–45.
29 L. Mayol, M. Biondi, L. Russo, B. M. Malle, K. Schwach-Abdellaoui and A. Borzacchiello, *Carbohydr. Polym.*, 2014, **102**, 110–116.
30 M. C. Koetting, J. T. Peters, S. D. Steichen and N. A. Peppas, *Mater. Sci. Eng., R*, 2015, **93**, 1–49.
31 R. Langer, *Acc. Chem. Res.*, 2000, **33**, 94–101.
32 L. Klouda, *Eur. J. Pharm. Biopharm.*, 2015, **97**, 338–349.
33 A. Chilkoti, M. R. Dreher, D. E. Meyer and D. Raucher, *Adv. Drug Delivery Rev.*, 2002, **54**, 613–630.
34 S. R. Van Tomme, G. Storm and W. E. Hennink, *Int. J. Pharm.*, 2008, **355**, 1–18.
35 H. Liu, J. Liu, C. Qi, Y. Fang, L. Zhang, R. Zhuo and X. Jiang, *Acta Biomater.*, 2016, **35**, 228–237.
36 M. P. Lutolf, *Integr. Biol.*, 2009, **1**, 235.
37 N. R. Cashman, H. D. Durham, J. K. Blusztajn, K. Oda, T. Tabira, I. T. Shaw, S. Dahrouge and J. P. Antel, *Dev. Dyn.*, 1992, **194**, 209–221.
38 C. J. Eggett, S. Crosier, P. Manning, M. R. Cookson, F. M. Menzies, C. J. McNeil and P. J. Shaw, *J. Neurochem.*, 2000, **74**, 1895–1902.
39 D. Elieh-Ali-Komi and M. R. Hamblin, *Int. J. Adv. Res.*, 2016, **4**, 411–427.
40 M. Amidi, E. Mastrobattista, W. Jiskoot and W. E. Hennink, *Adv. Drug Delivery Rev.*, 2010, **62**, 59–82.
41 C. M. Lehr, J. A. Bouwstra, E. H. Schacht and H. E. Junginger, *Int. J. Pharm.*, 1992, **78**, 43–48.
42 M. Dash, F. Chiellini, R. M. Ottenbrite and E. Chiellini, *Prog. Polym. Sci.*, 2011, **36**, 981–1014.
43 C. Tonda-Turo, F. Ruini, M. Ramella, F. Boccafoschi, P. Gentile, E. Gioffredi, G. Falvo D'Urso Labate and G. Ciardelli, *Carbohydr. Polym.*, 2017, **162**, 82–92.
44 C. M. Valmikinathan, V. J. Mukhatyar, A. Jain, L. Karumbaiah, M. Dasari and R. V. Bellamkonda, *Soft Matter*, 2012, **8**, 1964–1976.
45 A. Chenite, M. Buschmann, D. Wang, C. Chaput and N. Kandani, *Carbohydr. Polym.*, 2001, **46**, 39–47.
46 H. Y. Zhou, L. J. Jiang, P. P. Cao, J. B. Li and X. G. Chen, *Carbohydr. Polym.*, 2015, **117**, 524–536.
47 J. Cho, M. C. Heuzey, A. Bégin and P. J. Carreau, *Biomacromolecules*, 2005, **6**, 3267–3275.
48 E. Assaad, M. Maire and S. Lerouge, *Carbohydr. Polym.*, 2015, **130**, 87–96.
49 Z. Huang, B. Yu, Q. Feng and S. Li, *Polym. Polym. Compos.*, 2011, **19**, 781–787.
50 F. Ruini, C. Tonda-Turo, V. Chiono and G. Ciardelli, *Biomed. Mater.*, 2015, **10**, 65002.

 This journal is © The Royal Society of Chemistry 2021

Open Access Article. Published on 28 September 2021. Downloaded on 1/21/2026 7:01:05 PM.
This article is licensed under a Creative Commons Attribution-NonCommercial 3.0 Unported Licence.

51 S. Johann, M. Dahm, M. Kipp, U. Zahn and C. Beyer, *J. Neuroendocrinol.*, 2011, **23**, 839–848.
52 O. Maier, J. Böhm, M. Dahm, S. Brück, C. Beyer and S. Johann, *Neurochem. Int.*, 2013, **62**, 1029–1038.
53 A. Stanzione, A. Polini, V. La Pesa, A. Romano, A. Quattrini, G. Gigli, L. Moroni and F. Gervaso, *Applied sciences-Basel*, 2020, **10**, 6550.
54 C. Ceccaldi, E. Assaad, E. Hui, M. Buccionyte, A. Adoungotchodo and S. Lerouge, *Macromol. Biosci.*, 2017, **17**, 1–10.
55 Y. B. Schuetz, R. Gurny and O. Jordan, *Eur. J. Pharm. Biopharm.*, 2008, **68**, 19–25.
56 M. Rahimnejad, T. Labonté-Dupuis, N. R. Demarquette and S. Lerouge, *Biomed. Mater.*, 2020, **16**, 015003.
57 Y. Alinejad, A. Adoungotchodo, E. Hui, F. Zehtabi and S. Lerouge, *Int. J. Biol. Macromol.*, 2018, **113**, 132–141.
58 B. V. Slaughter, S. S. Khurshid, O. Z. Fisher, A. Khademhosseini and N. A. Peppas, *Adv. Mater.*, 2009, **21**, 3307–3329.
59 C. F. Guimarães, L. Gasperini, A. P. Marques and R. L. Reis, *Nat. Rev. Mater.*, 2020, **5**, 351–370.